

OPTICS OF NANOPARTICLES

PACS numbers: 78.67.Bf; 78.67.Sc; 71.35.Aa; 73.20.Mf
DOI: 10.1070/QE2013v043n11ABEH015180

Optical properties of three-layer metal-organic nanoparticles with a molecular J-aggregate shell

V.S. Lebedev, A.S. Medvedev

Abstract. **This paper examines the optical properties of two types of spherical three-component nanoparticles: (1) particles comprising a metallic core, outer organic dye J-aggregate shell and passive intermediate layer and (2) metallic nanoshells having an insulator or semiconductor core and coated with a molecular J-aggregate layer. The two types of nanoparticles are shown to differ significantly in the behaviour of electromagnetic fields and photoabsorption spectra. As a result of additional possibilities to control the magnitude and nature of the coupling between Frenkel excitons and localised surface plasmons in these systems, the spectral properties of the three-layer particles have radically new inherent features in comparison with earlier studied metal/J-aggregate bilayer particles. In the case of J-aggregate-coated metallic nanoshells, particular attention is paid to the strong plasmon–exciton coupling regime, which takes place when the plasmon resonance frequency of the nanoshell approaches the centre frequency of the J-band of the dye forming the outer layer of the particle.**

Keywords: *nanophotonics, hybrid nanoparticles, metallic nanoshells, molecular J-aggregates, semiconductor core, localised plasmons, plasmon–exciton coupling, photoabsorption spectra.*

1. Introduction

At present, leading research centres are carrying out intensive studies aimed at developing next-generation photonic and optoelectronic devices that will take advantage of subwavelength optics and quantum-confinement, nonlinear and plasmonic phenomena, including research in the fields of nanolasers [1–3], organic light emitting diodes with embedded quantum dots [4, 5], optical switches and memory elements [6, 7], photovoltaic cells [8], nanowaveguides [9, 10] and converters of light to fields localised on a nanoscale [11, 12]. A great deal of attention is paid to creating components of nanophotonic integrated circuits [13]. Advances in these areas require the engineering and characterisation of new materials with controlled optical properties. A promising approach for solving a number of problems is to use systems composed of metallic nanoparticles and molecules or molecular complexes, including ordered cyanine dye J-aggregates, in which electronic excitations of individual molecules become delocalised owing to the translational order in the system and form Frenkel excitons. Hybrid metal-organic nanoparticles, as well as molecules and molecular complexes situated near a metal surface or near metallic nanostructures of various shapes and dimensions, possess unique optical properties. Some of them are a consequence of the rapid increase in local field near the surface of a metallic particle interacting with an external electromagnetic field. Local fields may change the electronic structure and properties of individual molecules, molecular complexes and J-aggregates [14]. Another group of effects originate from electromagnetic coupling between a molecular subsystem and surface plasmons in a metal. This results in new hybrid states of the system, whose optical properties differ from the properties of any of its components. The effect is particularly pronounced when there is strong coupling between plasmons and Frenkel excitons of molecular J-aggregates.

Until recently, the interaction of Frenkel excitons with surface plasmons was studied mainly in hybrid metal-organic nanostructures with a planar geometry, for example, in thin metallic films coated with molecular J-aggregates, and in organic semiconductors (cyanine dyes embedded in a polymer matrix) applied to a metallic film [15–18]. In such cases, Frenkel excitons are electromagnetically coupled to plasmons propagating along a planar metal–insulator or metal–semiconductor interface. At the same time, Kometani et al. [19] demonstrated cyanine dye J-aggregation on a spherical surface of noble-metal nanoparticles in an aqueous solution. Similar metal/J-aggregate nanoparticles were then synthesised and characterised in a number of studies [20–28]. This opened up the possibility of gaining insight into coherent coupling between molecular excitons and localised plasmons.

The key features of the absorption spectra of small ($r \lesssim 10$ nm) silver and gold nanoparticles coated with J-aggregates of the cyanine dye TC (3,3′-disulfopropyl-5,5′-dichlorothiacyanine sodium salt) were interpreted in the quasi-static approximation using an analytical model for the dipole polarisability of two concentric spheres [23, 24, 27–29]. The optical properties of metal/J-aggregate bilayer nanoparticles were calculated and analysed in detail in wide ranges of geometric parameters of the nanoparticles and dielectric constants of the constituent materials using generalised Mie theory [30]. In addition, we provided an explanation for the coupling between Frenkel excitons in the J-aggregates shell of a particle and dipole and multipole plasmons localised in its core.

Several recent reports described the synthesis of spherical [31, 32], rod-shaped [33, 34] and dumbbell-like [35] three-layer nanostructures composed of a gold or silver core, outer dye

V.S. Lebedev P.N. Lebedev Physics Institute, Russian Academy of Sciences, Leninsky prosp. 53, 119991 Moscow, Russia; Moscow Institute of Physics and Technology (State University), Institutskii per. 9, 141700 Dolgoprudnyi, Moscow region, Russia; e-mail: vlebedev@sci.lebedev.ru;
A.S. Medvedev Moscow Institute of Physics and Technology (State University), Institutskii per. 9, 141700 Dolgoprudnyi, Moscow region, Russia; e-mail: primefc@gmail.com

Received 20 March 2013; revision received 19 June 2013
Kvantovaya Elektronika **43** (11) 1065–1077 (2013)
Translated by O.M. Tsarev

J-aggregate shell and passive intermediate layer. The objectives of this work were to theoretically analyse the optical properties of spherical three-layer nanoparticles and investigate the field distribution in the particles and around them. The spatial structure of fields and absorption cross sections were studied for particles comprising a noble-metal (Ag) core, outer cyanine dye [TC, OC, NK2567 (Fig. 1)] J-aggregate layer and insulator layer in between [self-organised organic layer of TMA: *N*,*N*,*N*-trimethyl(11-mercaptoundecyl)ammonium chloride]. Calculations were performed in wide ranges of wavelengths and geometric parameters of the system within generalised Mie theory for three concentric spheres, with allowance for the size effect on the dielectric function of the metallic core. We also considered the limiting case of small three-layer nanoparticles, where the quasi-static approximation is applicable.

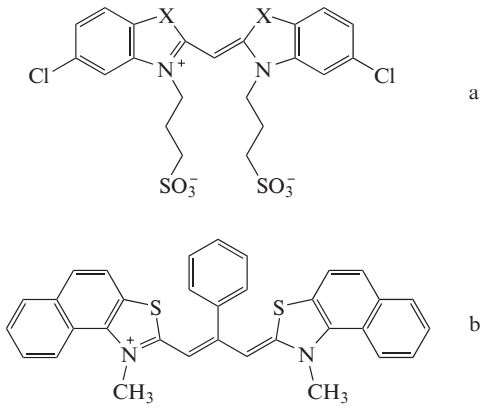

Figure 1. Molecular structures of the cyanine dyes studied: (a) TC (X = S, 3,3′-disulfopropyl-5,5′-dichlorothiacyanine sodium salt), OC (X = O, 3,3′-disulfopropyl-5,5′-dichlorooxacyanine triethylammonium salt), (b) NK2567 (2,2′-dimethyl-8-phenyl-5,5′,6,6′-dibenzothiacarbocyanine chloride).

Research interest in such three-layer nanostructures stems from the fact that the intermediate insulator layer offers an additional possibility to significantly control the nature and magnitude of the electromagnetic coupling between the J-aggregate shell and metallic core. Accordingly, in contrast to metal/J-aggregate bilayer nanoparticles, there is an additional possibility to control plasmon–exciton coupling in metal-organic nanosystems and, as a consequence, to significantly tune their optical properties, including the efficiency and spectral distribution of light absorption and scattering. This is important for basic research into the effect of molecular J-aggregates on the spectroscopic properties of hybrid nanoparticles and nanomaterials [36, 37] and may find application in organic optoelectronics and nanophotonics [38, 39], in particular, in plasmonic solar-cell engineering [40]. Moreover, in contrast to metal/J-aggregate two-component nanoparticles, three-component nanoparticles having a passive intermediate layer between their metallic core and outer J-aggregate shell can not only effectively absorb and scatter light but also photoluminesce in the visible range [32]. This is of interest for a number of applications in the field of organic light emitting diodes that utilise plasmonic effects [41–43]. Analysis in this study demonstrates that plasmon– exciton coupling effects in three-layer nanoparticles and their spectral characteristics have specific features that distinguish them from both molecular J-aggregates on a flat surface of a bulk metal and J-aggregates applied directly to the surface of a metallic particle.

In addition to the above metal-organic nanostructures, Fofang et al. [36] synthesised SiO_2/Au/J-aggregate three-component nanoparticles using so-called metallic nanoshells (SiO_2/Au), which were coated with an outer layer of cyanine dye molecular J-aggregates. The structure and optical properties of two-component nanoshells comprising an insulator core and noble-metal layer have been the subject of extensive studies (see e.g. [44–48] and references therein). It has been shown that, varying the ratio of the shell thickness to the core radius, one can tune plasmon frequencies of the hybrid system in the visible and near-IR spectral regions. The tunability of plasmon resonance frequencies in such systems makes them attractive for efficient solar power conversion [49] and a number of medical applications [50]. In this study, we examine the optical properties of insulator/metal/J-aggregate (SiO_2/Ag/J-aggregate) three-layer particles and metallic nanoshells having an outer J-aggregate layer and semiconductor core instead of a silica core (for example, Si/Ag/J-aggregate and GaN/Ag/J-aggregate). The high dielectric permittivity ε of the semiconductor core of such particles ($\mathrm{Re}\varepsilon \sim 10-20$) has a significant effect on their spectral properties, in particular on the frequency and width of the hybrid modes of the system. Research interest in three-layer (insulator/metal/J-aggregate and semiconductor/metal/J-aggregate) nanostructures is also aroused by the fact that, varying the geometry of the system, one can tune the plasmon resonance frequency of the metallic nanoshell to the centre frequency of the J-band of the dye that forms the outer layer of the particle. This offers a unique possibility to study interaction between localised surface plasmons and Frenkel excitons in the strong coupling regime.

2. Basic formulas for the light absorption and scattering cross sections of three-component particles

The absorption and scattering spectra of metallic-core hybrid nanoparticles whose size exceeds the Fermi wavelength of electrons in metals, $\lambda_F \sim 1$ nm, can be quantitatively described within the classical electrodynamics of continuous media. When local dielectric functions of the constituent materials of a particle are used, the exact solution to the problem of light absorption and scattering is a generalisation of standard Mie theory [51] for a uniform sphere (see also Ref. [52]) to multilayer spherical particles, subject to appropriate boundary conditions. This approach was developed in a number of studies. First, standard Mie theory was generalised to particles having one additional outer layer in Refs [53, 54]. Generalisation to an arbitrary number of layers was performed in Ref. [55] using the matrix formalism and in Refs [56, 57] using recurrent relations for scattering coefficients of a multilayer spherical particle. The theory thus developed was used in a number of studies to calculate and analyse the optical properties of spherical composite nanoparticles of various compositions and sizes (see e.g. Refs [30, 36, 44, 58–61]).

Figure 2 shows a schematic representation of the three-component particles under consideration. The materials of the concentric spherical layers are taken to be uniform and isotropic, with frequency-dependent complex permittivities ε_1, ε_2 and ε_3 (the permittivity of the metallic component is

size-dependent as well) and magnetic permeabilities $\mu_1 = \mu_2 = \mu_3 = 1$. The particle is surrounded by a medium of dielectric permittivity $\varepsilon_h(\omega)$ and magnetic permeability $\mu_h = 1$. A monochromatic plane wave incident on the particle, $E \propto \exp(-i\omega t + ik_h z)$, is partially scattered and absorbed. The general expressions for the light absorption and scattering cross sections (σ_{abs} and σ_{scat}) of a multilayer spherical particle and its total extinction cross section (σ_{ext}) have the form [52]

$$\sigma_{abs} = \frac{\pi}{2k_h^2}\sum_{n=1}^{\infty}[(2n+1)(2-|2a_n-1|^2-|2b_n-1|^2)], \quad (1)$$

$$\sigma_{scat} = \frac{\pi}{2k_h^2}\sum_{n=1}^{\infty}[(2n+1)(|a_n|^2+|b_n|^2)], \quad (2)$$

$$\sigma_{ext} = \frac{\pi}{2k_h^2}\sum_{n=1}^{\infty}(2n+1)\,\mathrm{Re}(a_n+b_n). \quad (3)$$

Here, a_n and b_n are the coefficients in the expansion of the transverse electric (TE) and transverse magnetic (TM) modes of the scattered wave, respectively; n is the multipole order; and $k_h = \omega\sqrt{\varepsilon_h}/c$ is the magnitude of the wave vector in the medium around the particle.

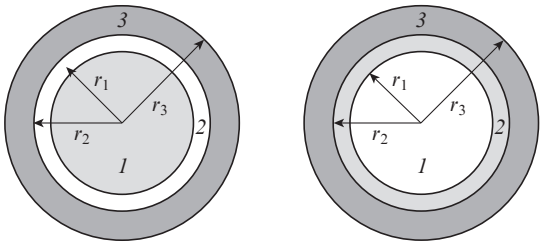

a b

Figure 2. Schematic of the structure of the nanoparticles under examination: (a) particle comprising (*1*) a metallic core, (*3*) outer J-aggregate shell and (*2*) passive insulator layer; (b) particle comprising (*1*) an insulator (semiconductor) core and (*2*) a metallic shell coated with (*3*) a J-aggregate.

In the case of three-component particles, the expressions obtained for the coefficients a_n and b_n by solving the system of equations subject to boundary conditions at $r = r_1$, $r = r_2$ and $r = r_3$ are rather cumbersome. For this reason, in contrast to the case of two-component particles [30], it is convenient to represent the coefficients a_n and b_n, corresponding to the contributions of the TE and TM modes, not as determinants but using recurrent relations:

$$a_n = \frac{X_n^{(a)}}{Y_n^{(a)}},\ b_n = \frac{X_n^{(b)}}{Y_n^{(b)}}. \quad (4)$$

For the TE modes, $X_n^{(a)}$ and $Y_n^{(a)}$ are given by

$$X_n^{(a)} = u_n(k_h r_3)[u_n'(k_3 r_3) + A_2 v_n'(k_3 r_3)] - \sqrt{\frac{\varepsilon_h}{\varepsilon_3}}\,u_n'(k_h r_3)[u_n(k_3 r_3) + A_2 v_n(k_3 r_3)], \quad (5)$$

$$Y_n^{(a)} = w_n(k_h r_3)[u_n'(k_3 r_3) + A_2 v_n'(k_3 r_3)] - \sqrt{\frac{\varepsilon_h}{\varepsilon_3}}\,w_n'(k_h r_3)[u_n(k_3 r_3) + A_2 v_n(k_3 r_3)]. \quad (6)$$

Here, $A_2 = -p/q$, where

$$p = u_n(k_3 r_2)[u_n'(k_2 r_2) + A_1 v_n'(k_2 r_2)] - \sqrt{\frac{\varepsilon_3}{\varepsilon_2}}\,u_n'(k_3 r_2)[u_n(k_2 r_2) + A_1 v_n(k_2 r_2)], \quad (7)$$

$$q = v_n(k_3 r_2)[u_n'(k_2 r_2) + A_1 v_n'(k_2 r_2)] - \sqrt{\frac{\varepsilon_3}{\varepsilon_2}}\,v_n'(k_3 r_2)[u_n(k_2 r_2) + A_1 v_n(k_2 r_2)]. \quad (8)$$

The final expressions for p, q, A_2, $X_n^{(a)}$, $Y_n^{(a)}$ and, hence, a_n can be obtained from Eqns (4)–(8) by substituting the explicit form of A_1, which can be expressed through spherical Riccati–Bessel [$u_n(z) = zj_n(z)$], Riccati–Neumann [$v_n(z) = zy_n(z)$] and Riccati–Hankel [$w_n(z) = zh_n^{(1)}(z)$] functions [where $j_n(z)$, $y_n(z)$ and $h_n^{(1)}(z)$ are spherical Bessel, Neumann and Hankel functions] and their derivatives with respect to their argument:

$$A_1 = \frac{u_n(k_2 r_1)\,u_n'(k_1 r_1) - \sqrt{\varepsilon_2/\varepsilon_1}\,u_n'(k_2 r_1)u_n(k_1 r_1)}{v_n(k_2 r_1)\,u_n'(k_1 r_1) - \sqrt{\varepsilon_2/\varepsilon_1}\,v_n'(k_2 r_1)u_n(k_1 r_1)}. \quad (9)$$

Similarly, the coefficients $b_n = X_n^{(b)}/Y_n^{(b)}$, determining the contributions of the TM modes to the absorption, scattering and extinction cross sections in (1)–(4), can be found using the relations

$$X_n^{(b)} = \sqrt{\frac{\varepsilon_h}{\varepsilon_3}}\,u_n(k_h r_3)[u_n'(k_3 r_3) + B_2 v_n'(k_3 r_3)] - u_n'(k_h r_3)[u_n(k_3 r_3) + B_2 v_n(k_3 r_3)], \quad (10)$$

$$Y_n^{(b)} = \sqrt{\frac{\varepsilon_h}{\varepsilon_3}}\,w_n(k_h r_3)[u_n'(k_3 r_3) + B_2 v_n'(k_3 r_3)] - w_n'(k_h r_3)[u_n(k_3 r_3) + B_2 v_n(k_3 r_3)]. \quad (11)$$

Here, $B_2 = -s/t$, where

$$s = \sqrt{\frac{\varepsilon_3}{\varepsilon_2}}\,u_n(k_3 r_2)[u_n'(k_2 r_2) + B_1 v_n'(k_2 r_2)] - u_n'(k_3 r_2)[u_n(k_2 r_2) + B_1 v_n(k_2 r_2)], \quad (12)$$

$$t = \sqrt{\frac{\varepsilon_3}{\varepsilon_2}}\,v_n(k_3 r_2)[u_n'(k_2 r_2) + B_1 v_n'(k_2 r_2)] - v_n'(k_3 r_2)[u_n(k_2 r_2) + B_1 v_n(k_2 r_2)]. \quad (13)$$

The coefficient B_1 in (12) and (13) can be found as

$$B_1 = \frac{\sqrt{\varepsilon_2/\varepsilon_1}\,u_n(k_2 r_1)\,u_n'(k_1 r_1) - u_n'(k_2 r_1)u_n(k_1 r_1)}{\sqrt{\varepsilon_2/\varepsilon_1}\,v_n(k_2 r_1)\,u_n'(k_1 r_1) - v_n'(k_2 r_1)u_n(k_1 r_1)}. \quad (14)$$

Thus, at an arbitrary relationship between the particle size and the wavelength of the light, the absorption, scattering and extinction cross sections can be evaluated using formulas (1)–(3) of generalised Mie theory and the above expressions for the coefficients a_n and b_n.

When the particle radius is much smaller that the wavelength of the light, we can use the dipole approximation of Mie theory. The expressions for the light absorption and scattering

cross sections of a composite particle can then be written in the form

$$\sigma_{abs}(\omega) = 4\pi k_h V \mathrm{Im}[\tilde{\alpha}(w)], \quad (15)$$

$$\sigma_{scat}(\omega) = \frac{8\pi}{3} k_h^4 V^2 |\tilde{\alpha}(w)|^2, \quad (16)$$

where $\tilde{\alpha} = \alpha/V$ is the effective polarisability per unit volume for a particle of volume V and polarisability α. The polarisability $\tilde{\alpha}$ of a uniform sphere is represented by the standard formula

$$\tilde{\alpha} = \frac{3}{4\pi} \frac{\varepsilon - \varepsilon_h}{\varepsilon + 2\varepsilon_h}. \quad (17)$$

For a hybrid particle consisting of N spherical layers and situated in a colloidal solution, ε should be replaced by an effective complex dielectric function $\varepsilon_N^{\mathrm{eff}}$ of the composite spherical system, which can be found in a known manner using recurrent relations. This allows the effective dipole polarisability of a three-layer particle, $\alpha_{eff}(\omega)$, to be determined. The relevant formulas for $\alpha_{eff}(\omega)$ were presented elsewhere [62].

In particular calculations of the absorption and scattering cross sections of metal/insulator/J-aggregate three-layer particles (Fig. 2a), the dielectric function $\varepsilon_1 \equiv \varepsilon_m(\omega, r_1)$ of the metallic core is described by us (like in the case of metal/J-aggregate bilayer particles [30]) with allowance for the contribution of free and bound electrons, $\varepsilon_m = \varepsilon_{intra} + \varepsilon_{inter}$, and for the size effect [63], which is due to free-electron scattering by the spherical interface between the metal and passive insulator layer. This effect leads to a substantial increase in free-electron attenuation factor, $\gamma_{intra}(r_1)$, with decreasing particle size and, hence, to a variation of ε_{intra} with both frequency ω and metallic core radius r_1. This becomes especially important when r_1 is much smaller than the electron mean free path l_∞ in a bulk metal.

A similar size effect plays a significant role in describing the optical properties of metallic nanoshells with an insulator (semiconductor) core when its metallic layer is thin enough. To take into account this effect in particular calculations of the absorption and scattering cross sections of the insulator/metal/J-aggregate or semiconductor/metal/J-aggregate three-layer particles under consideration (Fig. 2b), the dielectric function $\varepsilon_2 \equiv \varepsilon_m(\omega, r_1, r_2)$ of the metallic layer is described by relation (17) from Ref. [59] (see also Refs [64–66]).

The dielectric function $\varepsilon_3 \equiv \varepsilon_J(\omega)$ of a molecular J-aggregate is given by

$$\varepsilon_J(\omega) = \varepsilon_J^\infty + \frac{f\omega_0^2}{\omega_0^2 - \omega^2 - i\omega\Gamma}, \quad (18)$$

where f is the reduced oscillator strength in the dye J-band; ω_0 is the centre frequency; Γ is the width of the Lorentzian profile; and ε_J^∞ is the permittivity far away from the centre of the J-band. These parameters of the dye J-aggregates under consideration are presented in Table 1. The permittivity of the passive intermediate layer (spacer) between the core and outer shell, $\varepsilon_2 \equiv \varepsilon_s$, is taken to be constant at 2.25, which corresponds to the organic material (TMA) used for this purpose in earlier experimental studies [31, 32]. The ambient medium in our calculations is water, whose permittivity varies only slightly across the visible range: $1.77 < \varepsilon_w < 1.82$ in the range 350–700 nm [67].

Table 1. Parameters of TC, OC and NK2567 cyanine dye J-aggregates.

Dye	ε_J^∞	ω_0/eV	λ_0/nm	f	Γ/eV	Ref.
TC	1	2.68	462.6	0.90	0.066	[22]
OC	1	3.04	407.2	0.01	0.039	[35]
NK2567	1	1.79	692.6	0.02	0.052	[39]

3. Absorption spectra and field structure for particles comprising a metallic core, outer J-aggregate shell and passive intermediate layer

Consider the optical properties of three-layer nanoparticles in aqueous solution. Each nanoparticle comprises a metallic core of radius r_1, an outer dye J-aggregate shell of thickness $l_J = r_3 - r_2$ and an intermediate insulator layer of thickness $l_s = r_2 - r_1$. When interacting with an external electromagnetic field, this layer acts as a passive insulator spacer between the two active layers of the nanoparticle: its core, where localised surface plasmons are excited, and its outer shell, with a Frenkel exciton trapped in it. The spacer thickness is an additional parameter (compared to metal/J-aggregate bilayer particles [30]) capable of influencing the magnitude and nature of core–shell electromagnetic coupling, thus modifying the spectral characteristics of the hybrid nanosystem. This can be illustrated by the example of Ag/TMA/TC nanoparticles, having a silver core, TC cyanine dye shell and TMA organic intermediate layer with a refractive index $n_s = 1.5$. To this end, we examine how their absorption spectrum varies with intermediate layer thickness l_s and consider distinctions from Ag/TC two-component nanoparticles.

Figure 3 presents calculated absorption spectra of particles with a constant core radius and shell thickness (r_1 = 10 nm, l_J = 3 nm), whereas the thickness of their intermediate layer, l_s, varies from 0 to 5 (Fig. 3a) and from 5 to 19 nm (Fig. 3b). It is seen that, with increasing l_s, one of the absorption peaks (the strongest) shifts slightly to shorter wavelengths, without changes in its height. The other peak shifts in the same direction, but its shift is considerably larger and its height drops to almost zero [Fig. 3a, spectrum (*8*)]. Further increasing l_s produces two extra peaks, whose position varies little and whose height increases. The position of the longer wavelength peak coincides with the peak position of the J-band of the TC dye. The central peak (obviously due to the plasmon resonance in the metallic core) continues to slightly shift to shorter wavelengths and decrease in height with increasing l_s (Fig. 3b). This indicates that the plasmon–exciton coupling becomes weaker with an increase in the thickness of the intermediate layer between the metallic core and J-aggregate shell.

Consider now the behaviour of absorption spectra in two distinct cases: (1) the core radius varies from 10 to 24 nm at constant intermediate layer and outer shell thicknesses: l_s = 1 nm, l_J = 3 nm (Fig. 4a); (2) the outer shell thickness varies (from 1 to 8 nm) at a constant core radius and constant intermediate layer thickness: r_1 = 10 nm, l_s = 1 nm (Fig. 4b). In both cases, the absorption spectra of the hybrid nanoparticles have two peaks in the visible range. With increasing core radius or J-aggregate layer thickness, the maximum absorption cross section increases, which is due to the increase in the total particle volume, $V = (4\pi/3)r_3^3$. The positions of the photoabsorption peaks are rather weak functions of core radius r_1 (Fig. 4a). By analogy with bilayer particles [30], this result can be accounted for by the fact that the optical properties of the three-layer system (in particular the positions of

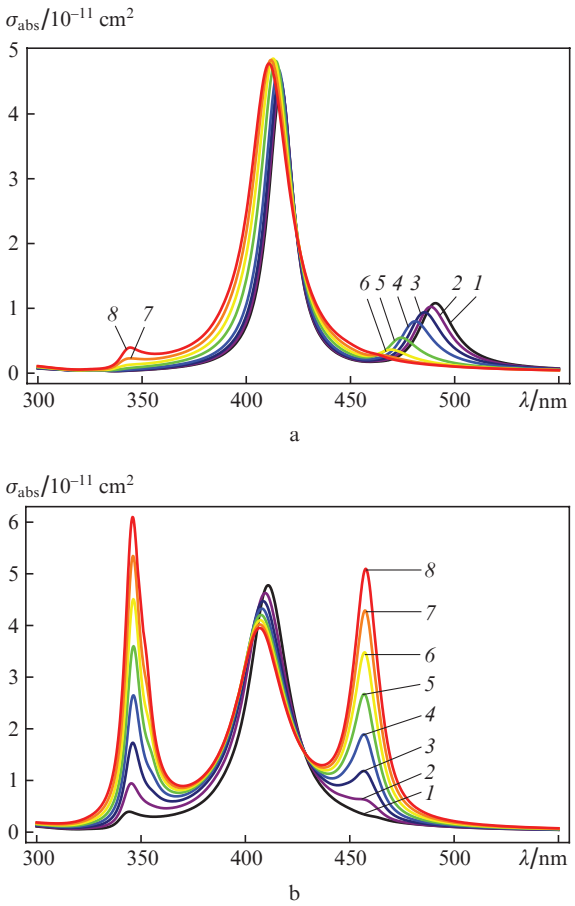

Figure 3. Light absorption cross section as a function of wavelength in vacuum for Ag/TMA/TC nanoparticles in aqueous solution: core radius r_1 = 10 nm, outer J-aggregate shell thickness l_J = 3 nm, intermediate layer thickness l_s = (a) (*1*) 0, (*2*) 0.2, (*3*) 0.5, (*4*) 1, (*5*) 2, (*6*) 3, (*7*) 4, (*8*) 5, (b) (*1*) 5, (*2*) 7, (*3*) 9, (*4*) 11, (*5*) 13, (*6*) 15, (*7*) 17, (*8*) 19 nm.

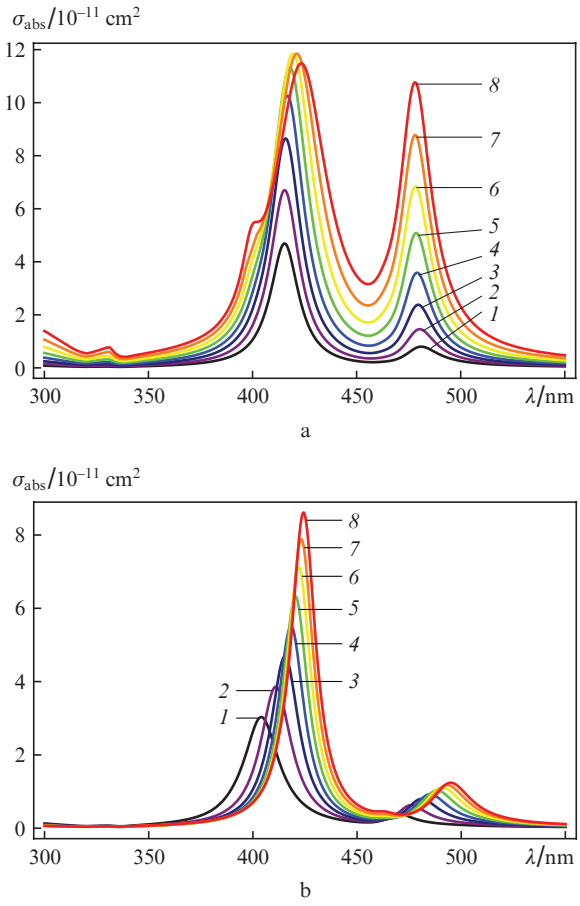

Figure 4. Light absorption cross section as a function of wavelength in vacuum for Ag/TMA/TC nanoparticles in aqueous solution: (a) inner shell thickness l_s = 1 nm, outer shell thickness l_J = 3 nm, core radius r_1 = (*1*) 10, (*2*) 12, (*3*) 14, (*4*) 16, (*5*) 18, (*6*) 20, (*7*) 22, (*8*) 24 nm; (b) r_1 = 10 nm, l_s = 1 nm, l_J = (*1*) 1, (*2*) 2, (*3*) 3, (*4*) 4, (*5*) 5, (*6*) 6, (*7*) 7, (*8*) 8 nm.

its spectral peaks) depend on the r_1/r_2 and r_2/r_3 ratios. In the former case (Fig. 4a), the two ratios vary little. In the latter (Fig. 4b), the outer particle radius varies from 12 to 19 nm, the r_1/r_2 ratio remains constant, and r_2/r_3 decreases from 0.92 to 0.56. Increasing the outer layer thickness l_J at constant r_1 and l_s leads to a considerable shift of the two peaks to longer wavelengths relative to the above case.

We also calculated the spatial field distribution within the composite particles under consideration and near their surface. Figure 5 presents the results for Ag/TMA/TC hybrid particles with a core radius r_1 = 10 nm, an outer shell thickness l_J = 3 nm and a varied passive layer thickness. In all cases, the incident light wavelength λ_0 corresponds to the peak position of the longer wavelength absorption peak (Fig. 3a) that is the most sensitive to changes in l_s. It follows from the present results that, at large intermediate layer thicknesses, the field enhancement region on the core surface overlaps very little with the organic shell. As l_s decreases, and the metallic core and organic shell approach each other, the $I/I_0 = |E/E_0|^2$ ratio (the ratio of the absolute square of the electric field, $|E|^2$, on the J-aggregate surface to that of the external field incident on the particle, $|E_0|^2$) increases. The I/I_0 ratio was determined to be 8.3, 10.3 and 12.2 at TMA organic intermediate layer thicknesses l_s = 5 nm, 2 nm and 0, respectively. At the same time, the electric field on the core surface becomes weaker with decreasing TMA layer thickness. For example, I/I_0 = 31.6, 21.0 and 3.1 at l_s = 5 nm, 2 nm and 0, respectively. Therefore, the maximum absorption cross section decreases.

Thus, we are led to conclude that, when the active layers of the hybrid system are spatially separated, the increase in local electromagnetic field in response to plasmon resonance excitation on the surface of the metallic core has a weaker effect on the field in the shell at a larger passive insulator layer thickness. This lends support to the above conclusion that the magnitude of the plasmon–exciton coupling between the metallic core and J-aggregate shell of a composite particle depends on insulator layer thickness l_s. At higher l_s values, the absorption peak position is less sensitive to changes in the geometry of the system (see Fig. 3b).

Compare now the calculation results to available experimental data. The dashed lines in Fig. 6 represent experimental data on light absorption in Ag/TMA bilayer particles and Ag/TMA/OC three-layer particles [32], and the solid lines represent the results obtained using the formulas given in Section 2. The core radius, intermediate layer thickness and outer J-aggregate shell thickness were set equal to r_1 = 7 nm, l_s = 1 nm and l_J = 4 nm. It is seen that the present theoretical calculation results are in satisfactory quantitative agreement with the experimental data presented in Fig. 6a. The calculation results for the Ag/TMA/OC three-layer particles reproduce all the main features of the photoabsorption spectrum. At the same time, there are quantitative discrepancies in the

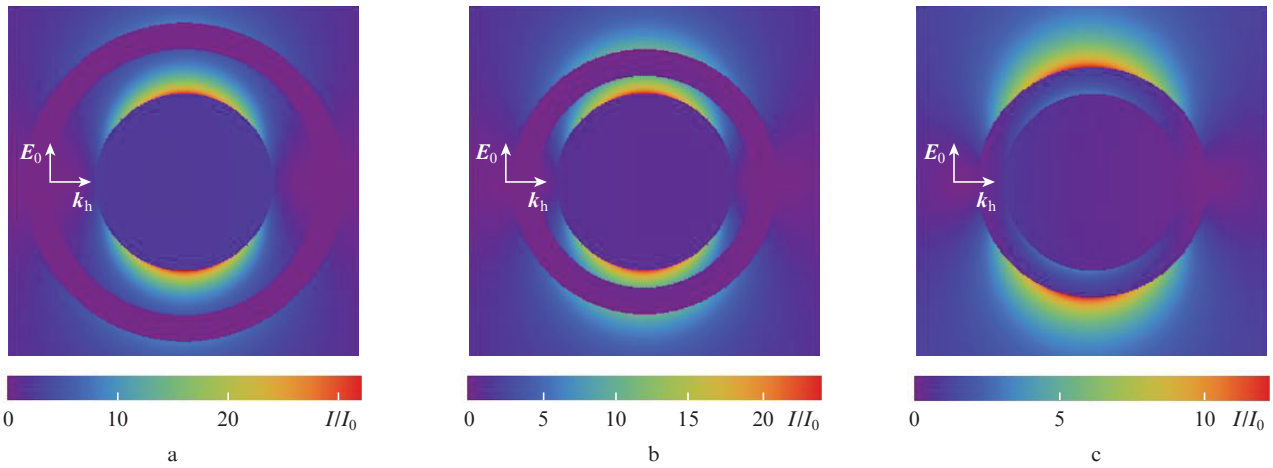

Figure 5. Near-field distributions of the absolute square of the electric field E_0 for Ag/TMA/TC nanoparticles with a core radius $r_1 = 10$ nm and outer shell thickness $l_J = 3$ nm at different insulator (TMA) layer thicknesses and incident light wavelengths: (a) $l_s = 5$ nm, $\lambda_0 = 468$ nm; (b) $l_s = 2$ nm, $\lambda_0 = 475$ nm; (c) $l_s = 0$, $\lambda_0 = 492$ nm.

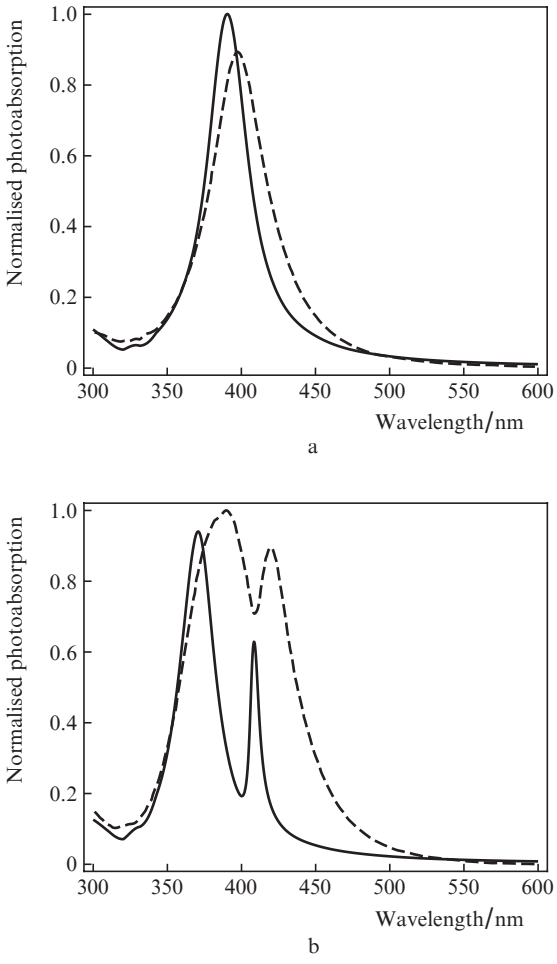

Figure 6. Absorption spectra calculated in this study for (a) Ag/TMA and (b) Ag/TMA/OC particles (solid lines) and corresponding experimental data [32] (dashed lines). Metallic core radius $r_1 = 7$ nm, intermediate layer thickness $l_s = 1$ nm, outer J-aggregate shell thickness $l_J = 4$ nm.

position and width of the peaks and in those of the dip in the spectral dependence of σ_{abs}. Possible reasons for the observed quantitative discrepancies between theory and experiment include the scatter in the size of composite nanoparticles in a real colloidal solution and uncertainty in the experimentally determined geometric parameters of the three-component particles [32], such as the core radius (r_1), outer shell thickness (l_J) and intermediate layer thickness (l_s). According to our calculations, the position and width of the absorption peaks of the hybrid nanoparticles are sufficiently sensitive to these parameters. Therefore, the observed scatter in the size of the composite particles may lead to inhomogeneous broadening of spectral peaks and changes in resonance frequencies.

4. Spectral characteristics of metallic nanoshells having an insulator or semiconductor core and coated with an outer molecular J-aggregate layer

Consider first the main differences between the absorption spectra of metallic nanoshells with an insulator core and metallic nanoshells coated with a molecular dye J-aggregate layer. Figure 7a presents the present calculation results for absorption spectra of SiO_2/Ag/J-aggregate three-layer nanoparticles in aqueous solution at an outer radius $r_3 = 38$ nm, varied core radius r_1 and, hence, varied thicknesses of the inner silver and outer J-aggregate layers. The radius r_1 increases from 28.8 to 33 nm in 0.6-nm steps [in going from spectrum (*1*) to spectrum (*8*)]. The inner layer thickness $l_s = r_2 - r_1$ and the outer layer thickness $l_J = r_3 - r_2$ decrease from 5.8 to 3 nm in 0.4-nm steps and from 3.4 to 2 nm in 0.2-nm steps, respectively. As constants determining the dielectric function $\varepsilon_J(\omega)$ [see Eqn (18)], we take parameters of the NK2567 dye molecular J-aggregate (Table 1). The calculation results for SiO_2/Ag bilayer particles are presented in Fig. 7b.

The absorption spectra of the three-layer particles and bilayer nanoshells differ primarily in the total number of spectral peaks. The spectra of the SiO_2/Ag/J-aggregate three-layer particles contain, in addition to the main spectral peak, located near the absorption peak of the SiO_2/Ag metallic nanoshells (no J-aggregate coating), another peak. Compared to the main peak, the additional peak shifts only slightly in response to changes in the geometric parameters of the particles within the above ranges. It is seen in Fig. 7a that the additional peak is located in the spectral range 650–700 nm [the right peak in spectra (*1*)–(*3*) and the left peak in spectra (*5*)–(*8*)],

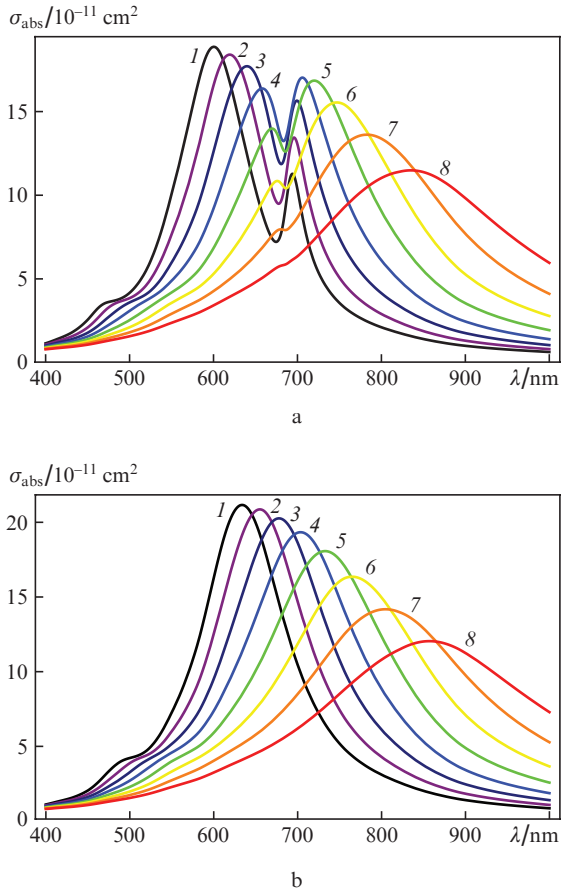

Figure 7. Absorption cross section σ_{abs} as a function of wavelength λ in vacuum for (a) SiO_2/Ag/NK2567 dye J-aggregate three-layer particles in aqueous solution and (b) SiO_2/Ag bilayer particles (no outer J-aggregate shell): outer radius $r_3 = 38$ nm; the core radius r_1 increases from (*1*) 28.8 to (*8*) 33 nm, the inner shell thickness l_s^{Ag} decreases from (*1*) 5.8 to (*8*) 3 nm, and the outer shell thickness l_J decreases from (*1*) 3.4 to (*8*) 2 nm.

whereas the main peak shifts from $\lambda \sim 600$ nm to $\lambda \sim 840$ nm. Note also that the additional peak is rather weak, but its height depends not only on the outer shell thickness but also on the position and width of the main peak. When the main peak is considerably shifted to longer wavelengths [Fig. 7a, spectrum (*8*)], the additional peak is so weak that it is hardly discernible. At the same time, the closer are the spectral peaks to each other, the stronger is the photoabsorption peak that emerges in the spectrum of the SiO_2/Ag/NK2567 three-layer hybrid particles because these have an outer J-aggregate layer [Fig. 7a, spectrum (*4*)].

Consider now how taking into account the size effect in describing the dielectric function of the metallic core influences the spectral properties of metallic nanoshells coated with cyanine dye J-aggregates (Fig. 8). For SiO_2/Ag/NK2567 particles with $r_1 = 25$ nm (core radius), $l_s^{Ag} = 5$ nm (metallic layer thickness) and $l_J = 3$ nm (outer organic shell thickness), taking into account the size effect [Fig. 8, spectrum (*1*)] increases the width of the plasmon peak by a factor of 2.4 and reduces its height by a factor of 1.7 with respect to spectrum (*2*). With increasing metallic shell thickness, the size effect on the width of the plasmon peak and the shape of the photoabsorption spectrum becomes weaker.

To illustrate the strong influence of the geometry of the systems under consideration on their absorption spectra, we

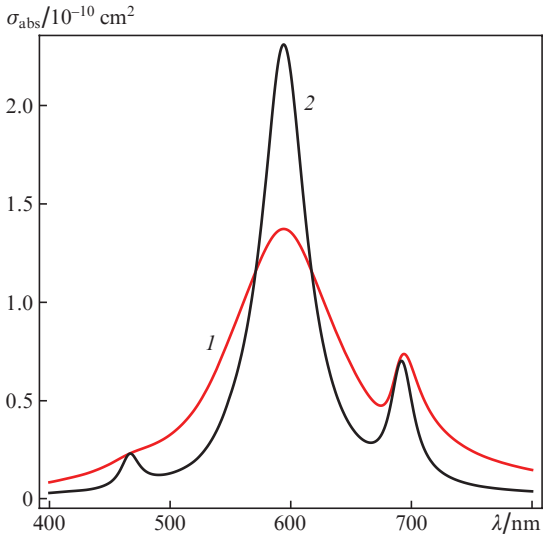

Figure 8. Photoabsorption spectra of SiO_2/Ag/NK2567 particles in aqueous solution: core radius $r_1 = 25$ nm, silver layer thickness $l_s^{Ag} = 5$ nm, outer J-aggregate shell thickness $l_J = 3$ nm; (*1*) calculation with allowance for the size effect in describing the dielectric function of the metallic core; (*2*) calculation with no allowance for the size effect.

present our calculation results for SiO_2/Ag/NK2567 three-layer nanoparticles with varied outer J-aggregate shell and metallic layer thicknesses. Figure 9 shows the absorption spectra of particles with a core radius $r_1 = 30$ nm and an inner shell thickness $l_s^{Ag} = 6$ nm. The outer shell thickness l_J varies from zero [spectrum (*1*)] (which corresponds to a SiO_2/Ag bilayer particle) to 18 nm [spectrum (*5*)]. It is seen that an increase in l_J leads to a considerable shift of the main peak in the photoabsorption spectrum of the three-layer particles to shorter wavelengths and reduces its height. It is worth noting that the effect is stronger at smaller outer shell thicknesses. For example, the difference in the position of the main absorption peak between the particles with $l_J = 1.5$ and 4.5 nm [spectra (*2*), (*3*)] is approximately equal to that between the particles with $l_J = 9$ and 18 nm [spectra (*4*), (*5*)]. In the former case (i.e. when the thickness l_J changes by 3 nm), the difference is 24 nm; in the latter (l_J changes by 9 nm), the difference

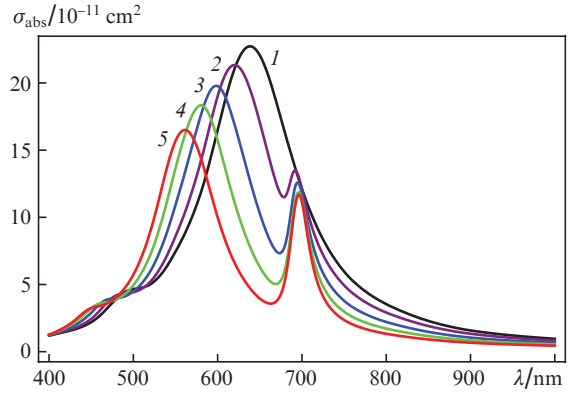

Figure 9. Photoabsorption spectra of SiO_2/Ag/NK2567 particles in aqueous solution: core radius $r_1 = 30$ nm, silver layer thickness $l_s^{Ag} = 6$ nm, outer J-aggregate shell thickness $l_J =$ (*1*) 0, (*2*) 1.5, (*3*) 4.5, (*4*) 9, (*5*) 18 nm.

is 22 nm. It is also worth pointing out that, in both cases, the maximum value of the absorption cross section σ_{abs} decreases by about 1.5×10^{-11} cm^2. At the geometric parameters under consideration, the additional spectral peak is weaker than the main peak and exhibits an opposite behaviour: with increasing l_J, it shifts to longer wavelengths and its height increases.

At the same time, the metallic layer thickness l_s^{Ag} has a stronger effect on the photoabsorption spectra of the insulator/metal/J-aggregate three-layer nanoparticles. It is seen in Fig. 10 that even a slight increase in l_s^{Ag} leads to a considerable shift of the main photoabsorption peak to shorter wavelengths. In the case under consideration, l_s^{Ag} varies from 3.5 [spectrum (*1*)] to 6 nm [spectrum (*5*)], whereas the core radius and outer shell thickness remain constant: r_1 = 30 nm and l_J = 3 nm. This corresponds to an almost twofold increase in the ratio of the silver layer thickness to the silica core radius, l_s^{Ag}/r_1. It is worth noting however that such an increase in l_s^{Ag}/r_1 has a considerably stronger effect on the peak position in and the shape of the photoabsorption spectrum than does an analogous twofold increase in the ratio of the outer J-aggregate shell thickness to the core radius, l_J/r_1.

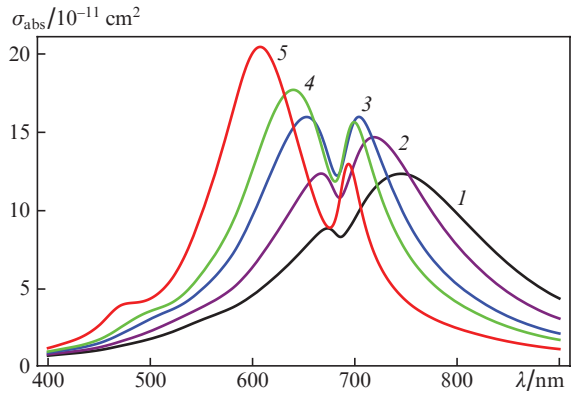

Figure 10. Photoabsorption spectra of SiO_2/Ag/NK2567 particles in aqueous solution: core radius r_1 = 30 nm, outer J-aggregate shell thickness l_J = 3 nm, inner metallic shell thickness l_s^{Ag} = (*1*) 3.5, (*2*) 4, (*3*) 4.6, (*4*) 5, (*5*) 6 nm.

Special mention should be given to the case (which occurs in the system under consideration at geometric parameters r_1 = 30 nm, l_s^{Ag} = 4.6 nm and l_J = 3 nm) where the main spectral peak is located near the additional peak, resulting from excitation of the outer molecular J-aggregate shell [Fig. 10, spectrum (*3*)]. The two peaks then become almost identical in height, and a characteristic dip is formed between them in the immediate vicinity of frequency ω_0. Further increasing the metallic layer thickness l_s^{Ag} shifts the main absorption peak to shorter wavelengths, whereas the additional peak shifts very little and decreases in height.

To examine in detail the situation where the photoabsorption peaks coincide in spectral position, we calculated the spatial field distribution within a SiO_2/Ag/NK2567 three-layer particle and near it using the following geometric parameters of the particle: insulator core radius r_1 = 30 nm, silver layer thickness l_s^{Ag} = 4.6 nm, shell thickness l_J = 3 nm [the parameters that were used in calculating spectrum (*3*) in Fig. 10]. The field calculation results for three incident light wavelengths are presented in Fig. 11. The wavelengths 651 and 703 nm (Figs 11a, 11c) correspond to absorption peaks of the composite nanoparticle, and the wavelength 684 nm (Fig. 11b) corresponds to a local minimum in the spectrum. It is seen that the field distributions in Figs 11b and 11c are similar. The electric field $\boldsymbol{E}$ increases mainly in the outer J-aggregate shell. The magnitude of $\boldsymbol{E}$ increases six to seven times, and the absolute square $|E|^2$ increases ~30 to 50 times. A drastically different field distribution was obtained at a wavelength of 651 nm, corresponding to the left absorption peak [Fig. 10, spectrum (*3*)]: the field varies little and is maximal in the insulator core of the hybrid particle.

To illustrate the contributions of the dipole term (n = 1) and higher multipole orders (n > 1) to the light absorption cross section of the SiO_2/Ag/NK2567 nanoparticles, Fig. 12 presents our σ_{abs} calculation results for various geometric parameters. Spectra (*1*) were obtained with allowance for the contribution of all the TM and TE modes in Eqn (1), and spectra (*2*), (*3*), (*4*) and (*5*) represent the contributions of the dipole (n = 1), quadrupole (n = 2), octupole (n = 3) and n = 4 terms in (1), respectively. At the geometric parameters used, the contribution of the quadrupole mode (n = 2) and higher multipole orders to the photoabsorption process becomes

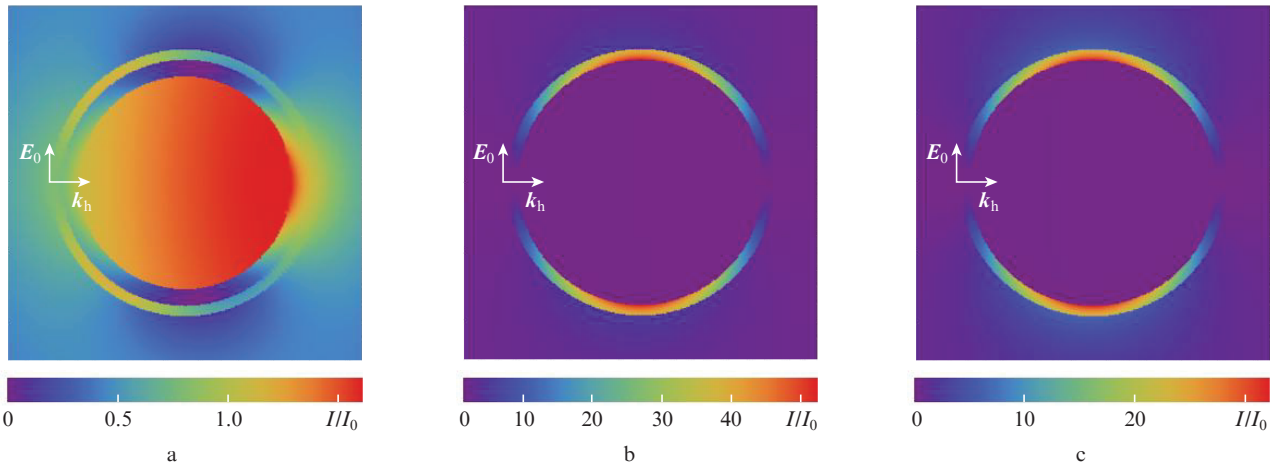

Figure 11. Near-field distributions of the absolute square of the electric field E_0 for SiO_2/Ag/NK2567 particles with a core radius r_1 = 30 nm, metallic layer thickness l_s^{Ag} = 4.6 nm and outer shell thickness l_J = 3 nm [the corresponding absorption spectrum (*3*) is presented in Fig. 10] at incident light wavelengths λ_0 = (a) 651, (b) 684 and (c) 703 nm.

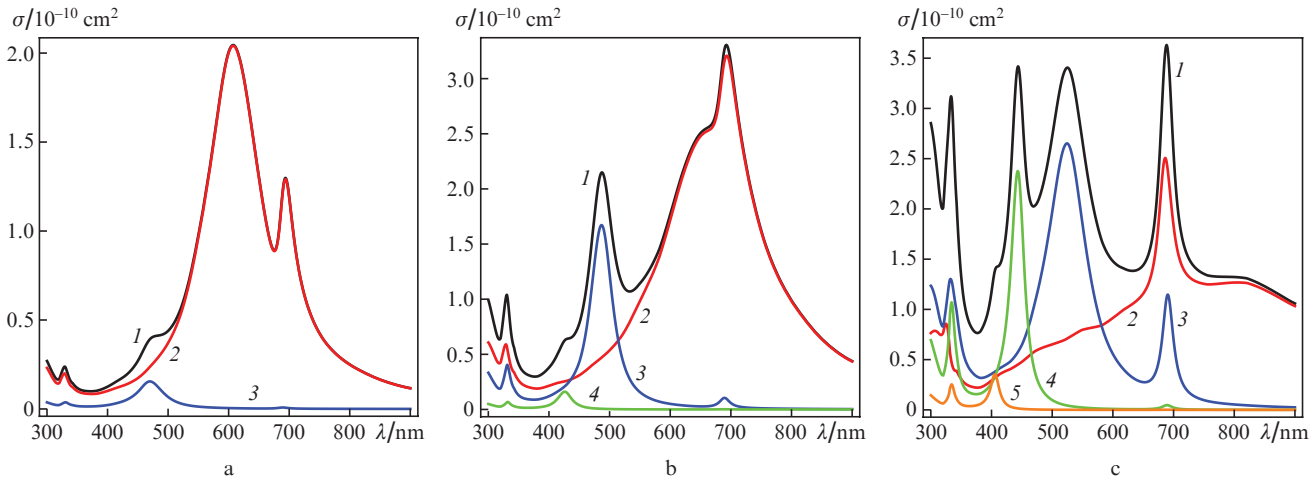

Figure 12. Calculated photoabsorption spectra of SiO_2/Ag/NK2567 particles with the following geometric parameters: (a) $r_1 = 30$ nm, $l_s^{Ag} = 6$ nm, $l_J = 3$ nm; (b) $r_1 = 50$ nm, $l_s^{Ag} = 10$ nm, $l_J = 5$ nm; (c) $r_1 = 80$ nm, $l_s^{Ag} = 16$ nm, $l_J = 8$ nm. Spectra (*1*) were obtained with allowance for the contribution of all the TM and TE modes in Eqn (1), and spectra (*2*), (*3*), (*4*) and (*5*) were obtained with allowance for the contributions of the first ($n = 1$), second ($n = 2$), third ($n = 3$) and fourth ($n = 4$) terms in (1), respectively.

first considerable and then rather large with increasing particle size. As a result, additional peaks emerge in the photoabsorption spectrum.

Figure 13 shows the photoabsorption, scattering and extinction spectra of the described systems with various geometric parameters. It follows from the present calculations that, at particle radii in the range ~30–40 nm, light scattering and absorption make comparable contributions to extinction, whereas in the range ~60–70 nm light scattering plays a key role. At small particle radii ($r_3 \lesssim 20$–25 nm), light extinction is determined primarily by the photoabsorption contribution. This follows, in particular, from the simple relations (15) and (16) in the quasi-static approximation.

Note that the choice of dye J-aggregates as outer shell materials has a strong effect on the optical properties of the hybrid systems under consideration. To demonstrate this, we calculated absorption spectra of SiO_2/Ag/J-aggregate three-layer nanoparticles using the optical constants ω_0, Γ and ε_J^∞ of two cyanine dyes (NK2567 and TC) (Table 1) in Eqn (18) (Fig. 14). The photoabsorption spectra in Fig. 14 are represented as functions of wavelength λ in vacuum and reduced oscillator strength f in the dye J-band. The value of f is varied from 0 to 2 to demonstrate how the efficiency of absorption in the outer J-aggregate shell influences the spectrum of the entire hybrid three-layer system. The point is that, depending on particular conditions (including the nanoshell material), f in the J-band may vary widely even for a given dye (see e.g. Ref. [23]). It also should be emphasised that the calculation result at $f = 0$ can be used to determine the plasmon resonance frequency of the nanoshell.

Thus, at high f values we can identify the peak corresponding to absorption in the SiO_2/Ag system. This can be done because at $f = 0$ the silver shell with an insulator core is coated with an additional outer layer having constant permittivity ε_J^∞, so that under such conditions the plasmon peak is the only peak in the absorption spectrum. It is seen in Fig. 14 that, with increasing f, the separation between the two new peaks increases. One of them corresponds to excitation of the J-aggregate shell. It shifts only slightly in response to changes in f (see e.g. the middle peak in Fig. 14b). The

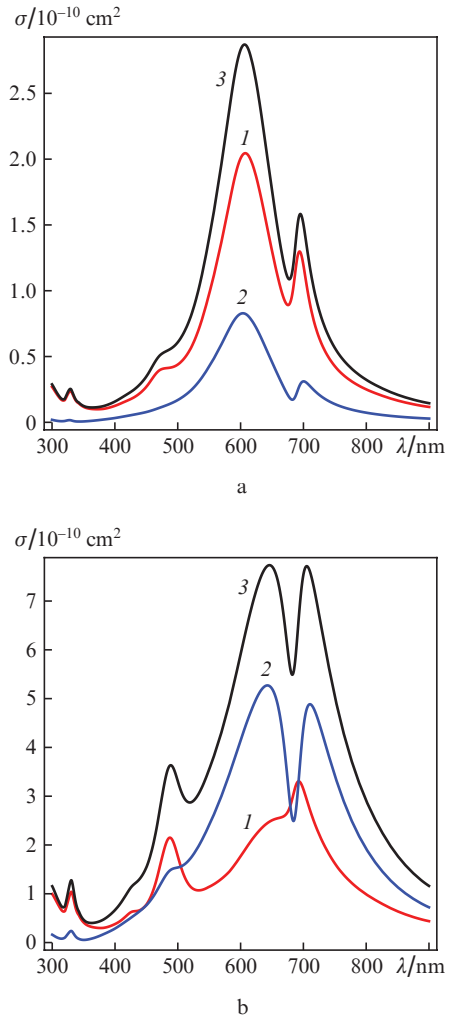

Figure 13. Calculated (*1*) photoabsorption, (*2*) scattering and (*3*) extinction spectra of SiO_2/Ag/NK2567 particles with the following geometric parameters: (a) $r_1 = 30$ nm, $l_s^{Ag} = 6$ nm, $l_J = 3$ nm; (b) $r_1 = 50$ nm, $l_s^{Ag} = 10$ nm, $l_J = 5$ nm.

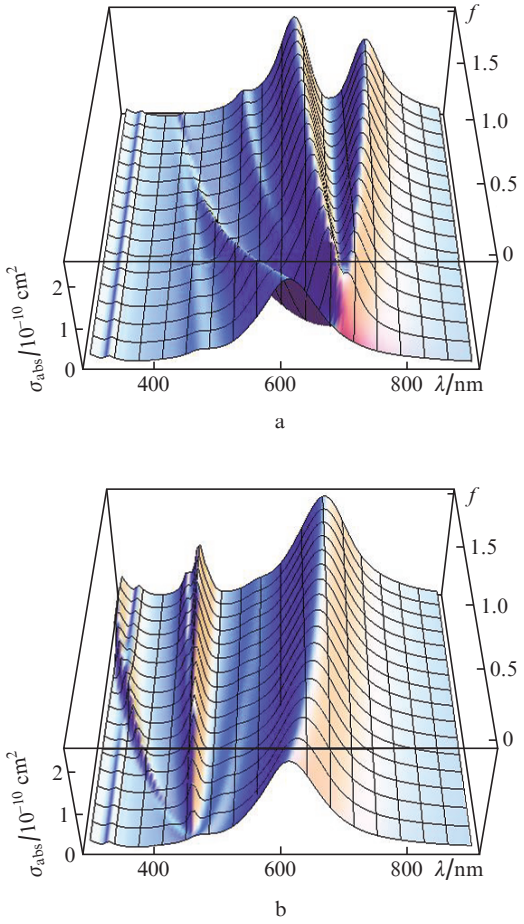

Figure 14. Photoabsorption cross section σ_{abs} as a function of wavelength λ in vacuum and reduced oscillator strength f in the dye J-band for SiO_2/Ag/J-aggregate three-layer nanoparticles (silica core and silver layer) in aqueous solution: $r_1 = 30$ nm, $l_s^{Ag} = 60$ nm, $l_J = 3$ nm; ω_0, Γ and ε_J^∞ in (18) are equal to those of (a) NK2567 and (b) TC dye J-aggregates (Table 1).

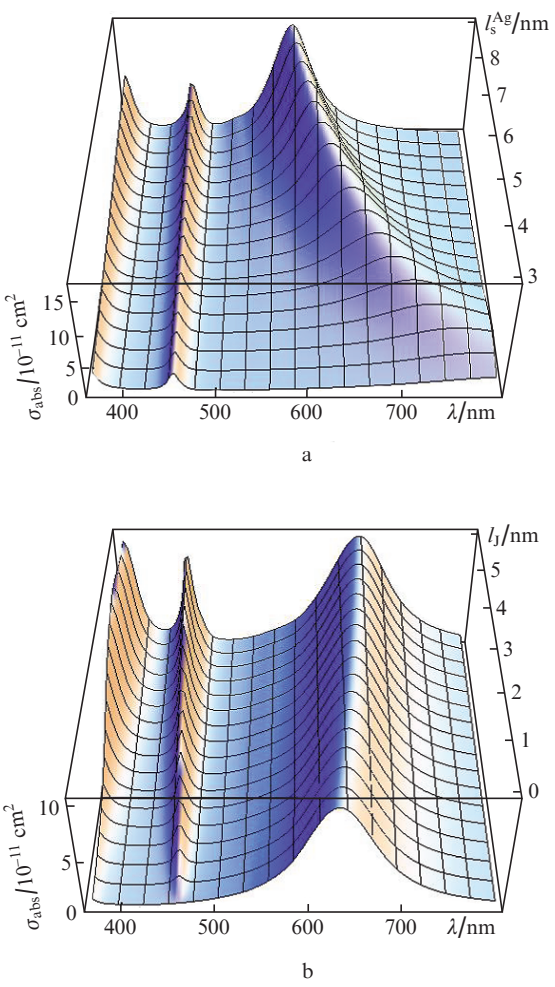

Figure 15. Absorption spectra of GaN/Ag/TC nanoparticles: (a) core radius $r_1 = 20$ nm, J-aggregate shell thickness $l_J = 3$ nm; (b) core radius $r_1 = 20$ nm, metallic shell thickness $l_s^{Ag} = 6$ nm.

other additional spectral peak results from interaction between a plasmon in the silver nanoshell and a Frenkel exciton in the outer J-aggregate layer. It is weaker than the other peaks, but its position is a strong function of f. The behaviour of the plasmon peak depends on its position relative to the other spectral peaks. If the plasmon resonance frequency ω_{res} is lower than ω_0 in (18), the corresponding peak shifts to longer wavelengths, whereas for $\omega_{res} > \omega_0$ the peak shifts to shorter wavelengths.

To describe the behaviour of the photoabsorption spectra of metallic nanoshells having a semiconductor core and coated with a cyanine dye J-aggregate, we calculated the corresponding cross sections σ_{abs} as functions of wavelength λ and silver layer thickness l_s^{Ag} (Fig. 15a) or as functions of λ and inner J-aggregate layer thickness l_J (Fig. 15b). It is seen in Fig. 15 that the peak corresponding to the plasmon resonance of the GaN/Ag nanoshell (right peak) experiences the strongest changes. With increasing silver shell thickness (Fig. 15a), it shifts markedly to shorter wavelengths. This would be expected because we vary the geometric parameters of the nanoshell itself, which have a strong effect on the position of the plasmon resonance peak of the bilayer nanoparticles. By contrast, varying the molecular dye J-aggregate shell thickness l_J (Fig. 15b) shifts the plasmon resonance peak to longer wavelengths, and the shift is smaller than that above. In both cases, the position of the absorption peak corresponding to J-aggregate shell excitation varies only slightly (middle peak in Fig. 15). As to the height of the spectral peaks, note that the absorption peak corresponding to excitation of the outer organic layer is the most sensitive to geometric parameters. Its height decreases with decreasing l_s^{Ag} and l_J (middle peak in Fig. 15a). At $l_J = 0$, this peak is missing, as would be expected.

Consider now photoabsorption spectra of substantially larger hybrid nanoparticles having a high-permittivity semiconductor core, e.g. consisting of crystalline silicon [68, 69]. Figure 16 shows calculated light absorption cross sections of Si/Ag/TC three-layer particles [spectrum (*1*)] with geometric parameters $r_1 = 60$ nm, $l_s^{Ag} = 12$ nm and $l_J = 6$ nm. The absorption spectra of such particles have a number of new features.

First, in contrast to that of the silica-core three-layer particles, the plasmon peak is shifted to the IR, far away from the absorption peaks of the J-aggregate shell ($\lambda = 462.6$ nm, Table 1). The behaviour of the photoabsorption spectrum in the range $\lambda = 800–1200$ nm is determined primarily by the dipole and quadrupole resonances of the inner silver nanoshell of the Si/Ag particle, with peaks at $\lambda = 1010$ and 825 nm,

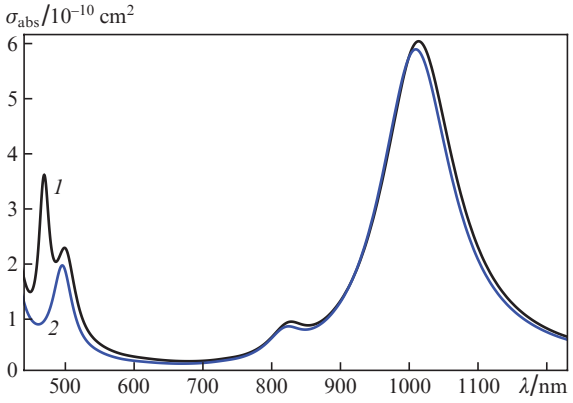

Figure 16. Absorption spectra of (*1*) Si/Ag/TC dye J-aggregate three-layer particles and (*2*) Si/Ag bilayer particles with a silicon core radius $r_1 = 60$ nm, metallic layer thickness $l_s^{Ag} = 12$ nm and J-aggregate shell thickness $l_J = 6$ nm.

respectively. The electromagnetic coupling of these plasmon resonances with the Frenkel exciton is rather weak, because they are markedly shifted from the centre wavelength λ_0 of the absorption band of the J-aggregate shell of the particle. Accordingly, coating the silver nanoshell of Si/Ag [Fig. 16, spectrum (*2*)] with a TC dye molecular J-aggregate has little effect on the shape of the photoabsorption spectrum in the region of the plasmon peaks.

Second, new photoabsorption peaks emerge in the visible range. In the Si/Ag/TC system under consideration, the peaks are located near $\lambda = 499$ and 469 nm. The peak at $\lambda = 499$ nm corresponds to the first Mie resonance for a silver nanoshell having a 60-nm silicon core (note that, in the case of analogous silica-core hybrid particles, the resonance would occur at a considerably greater core radius). The nearby peak of the three-layer particle at $\lambda = 469$ nm is due to light absorption by the external J-aggregate shell of the Si/Ag/TC particle. It is slightly shifted from the centre of the absorption band of the TC dye J-aggregate.

5. Conclusions

We have calculated the light absorption and scattering cross sections of two types of three-layer nanoparticles: particles having a metallic (Ag) core and a cyanine dye (TC) J-aggregate shell, separated by a passive organic (TMA) layer, and metallic nanoshells having an insulator (SiO_2) or semiconductor (GaN, Si) core and coated with J-aggregates of different cyanine dyes (NK2567, TC or OC). Calculations were performed in wide ranges of geometric parameters of the particles and incident light wavelengths.

One distinction of the former type of system from earlier studied metal/J-aggregate bilayer particles [30] is the presence of a passive intermediate layer. It has been shown that varying the thickness l_s of this layer, which ensures spatial separation between the surface of the metallic core of the particle and the molecular dye J-aggregate, produces significant changes in absorption spectrum in comparison with earlier studied metal/ J-aggregate bilayer particles (Fig. 3). Changes occur not only in the relative position and relative height of the peaks but also in the total number of spectral peaks. At small passive insulator (TMA) spacer thicknesses (l_s), varying the other geometric parameters (metallic core radius r_1 and J-aggregate shell thickness l_J) has a significant effect on the spectral properties of the system. At large intermediate layer thicknesses (i.e. when the active components of the hybrid particle are spatially separated), the photoabsorption and light scattering cross sections depend largely on the total particle size and vary only slightly with r_1 and l_J at a constant outer radius. This suggests that the additional intermediate layer changes the nature of plasmon–exciton coupling in such hybrid systems. On the whole, the present results demonstrate that the introduction of a passive intermediate layer offers an additional possibility to control the optical properties of composite nanosystems. Calculation results qualitatively reproduce all the main experimentally observed features of absorption spectra (Fig. 6). Moreover, calculations yield reasonable quantitative results.

The latter type of three-component particle is convenient for studies of metal-organic nanosystems in the strong plasmon–exciton coupling regime owing to the possibility of widely varying the spectral properties of the nanoshell and tuning its plasmon resonance frequency to the peak absorption frequency of the J-band of the outer organic shell (Fig. 7). The strong coupling regime takes place when the peak absorption wavelength λ_0 of the dye J-band approaches the plasmon resonance wavelength λ_{res}. Near the maximum of the dye J-band ($\lambda \sim \lambda_0$), this results in a well-defined spectral minimum and two photoabsorption peaks, similar in height, of the hybrid particle. Their heights are sensitive to geometric parameters of the system (Fig. 10). The response of the spectra to changes in the optical constants of the outer shell (e.g. the reduced oscillator strength f in the dye J-band) depends significantly on the relationship between the wavelengths λ_{res} and λ_0 (Fig. 14). If the plasmon resonance wavelength λ_{res} in the metallic nanoshell is shorter than the exciton excitation wavelength λ_0 in the J-aggregate shell, an increase in f causes the corresponding plasmon peak to shift to shorter wavelengths. For $\lambda_{res} > \lambda_0$, this absorption peak of the hybrid particle shifts to longer wavelengths.

It has also been shown that, in contrast to the case of small SiO_2/Ag/J-aggregate particles ($r_3 \lesssim 25-30$ nm), whose absorption cross section is determined primarily by the electric dipole contribution, the absorption spectra of hybrid nanoparticles with a radius $r_3 \gtrsim 50-60$ nm are significantly contributed by the interaction of Frenkel excitons with both dipole and multipole plasmons (Fig. 12). In this size range, the contribution of light scattering to the total extinction cross section first becomes comparable to the photoabsorption contribution and then prevails (Fig. 13).

In addition, we studied the optical properties of metallic nanoshells having a semiconductor core and coated with cyanine dye J-aggregates. Using the GaN/Ag/TC composite system as an example, we have shown that the spectral position of the absorption peak of the silver nanoshell is a strong function of its thickness and the outer organic shell thickness (Fig. 15). The absorption spectrum of Si/Ag/TC particles, with a high-permittivity core, have characteristic features even at relatively small core radii ($r_1 = 60$ nm). The shorter wavelength features are due to excitation of the first Mie resonance in the silicon core, near the absorption band of the outer hybrid shell (Fig. 16). Moreover, in contrast to those of analogous silica-core three-layer particles, the dipole and quadrupole plasmon peaks are shifted to the IR spectral region.

Acknowledgements. This work was supported by the Russian Foundation for Basic Research (Grant No. 12-02-00713-a), the RF Ministry of Education and Science (federal targeted programmes, Agreement Nos 8576 and 8396) and the Physical Sciences Division of the Russian Academy of Sciences (programmes 'Fundamental Optical Spectroscopy and Its Applications' and 'Fundamental Aspects of the Physics and Technology of Semiconductor Lasers As Cornerstones of Photonics and Quantum Electronics').

References

1. Zheludev N.I., Prosvirnin S.L., Papasimakis N., Fedotov V.A. *Nat. Photonics*, **2**, 351 (2008).
2. Protsenko I.I. *Usp. Fiz. Nauk*, **182**, 1116 (2012).
3. Yannopapas V., Psarobas I.E. *J. Opt.*, **14**, 035101 (2012).
4. Zhang Y.Q., Cao X.A. *Appl. Phys. Lett*., **97**, 253115 (2010).
5. Vashchenko A.A., Lebedev V.S., Vitukhnovskii A.G., Vasiliev R.B., Samatov I.G. *Pis'ma Zh. Eksp. Teor. Fiz*., **96**, 118 (2012) [*JETP Lett*., **96**, 113 (2012)].
6. Yan R., Gargas D., Yang P. *Nat. Photonics*, **3**, 569 (2009).
7. Agrawal A., Susut C., McMorran B., Stafford G., Lezec H., Talin A.A. *Nano Lett.*, **11**, 2774 (2011).
8. Atwater H.A., Polman A. *Nat. Mater.*, **9**, 205 (2010).
9. Barnes W. *J. Opt. A: Pure Appl. Opt.*, **8**, S87 (2006).
10. Kuznetsova T.I., Lebedev V.S. *Phys. Rev. E*, **78**, 016607 (2008).
11. Kuznetsova T.I., Lebedev V.S. *Pis'ma Zh. Eksp. Teor. Fiz.*, **79**, 70 (2004) [*JETP Lett*., **79**, 2, 62 (2004)].
12. Kuznetsova T.I., Lebedev V.S. *Phys. Rev. B*, **70**, 035107 (2004).
13. Ohtsu M. (Ed.) *Progress in Nano-Electro-Optics V: Nanophotonic Fabrications, Devices, Systems, and Their Theoretical Bases* (Berlin – Heidelberg – New York: Springer-Verlag, 2011).
14. Watanabe K., Menzel D., Nilius N., Freund H.-J. *Chem. Rev*., **106**, 4301 (2006).
15. Bellessa J., Bonnand C., Plenet J.C. *Phys. Rev. Lett*., **93**, 036404 (2004).
16. Bonnand C., Bellessa J., Plenet J.C. *J. Non-Cryst. Solids*, **352**, 1683 (2006).
17. Symonds C., Bonnand C., Plenet J.C., Bréhier A., Parashkov R., Lauret J.S., Deleporte E., Bellessa J. *New J. Phys.*, **10**, 065017 (2008).
18. Cade N.I., Ritman-Meer T., Richards D. *Phys. Rev. B*, **79**, 241404 (2009).
19. Kometani N., Tsubonishi M., Fujita T., Asami K., Yonezawa Y. *Langmuir*, **17**, 578 (2001).
20. Sato T., Tsugawa F., Tomita T., Kawasaki M. *Chem. Lett.*, **30**, 402 (2001).
21. Hranisavljevic J., Dimitrijevic N.M., Wurtz G.A., Wiederrecht G.P. *J. Am. Chem. Soc.*, **124**, 4536 (2002).
22. Wurtz G.A., Hranisavljevic J., Wiederrecht G.P. *J. Microsc.*, **210**, 340 (2003).
23. Wiederrecht G.P., Wurtz G.A., Hranisavljevic J. *Nano Lett*., **4**, 2121 (2004).
24. Wiederrecht G.P., Wurtz G.A., Bouhelier A. *Chem. Phys. Lett.*, **461**, 171 (2008).
25. Zhang J., Lakowicz J.R. *J. Phys. Chem. B*, **109**, 8701 (2005).
26. Uwada T., Toyota R., Masuhara H., Asahi T. *J. Phys. Chem. C*, **111**, 1549 (2007).
27. Lebedev V.S., Vitukhnovsky A.G., Yoshida A., Kometani N., Yonezawa Y. *Colloids Surf. A: Physicochem. Eng. Aspects*, **326**, 204 (2008).
28. Lebedev V.S., Medvedev A.S., Vasil'ev D.N., Chubich D.N., Vitukhnovsky A.G. *Kvantovaya Elektron*., **40**, 246 (2010) [*Quantum Electron*., **40**, 246 (2010)].
29. Medvedev A.S., Lebedev V.S. *Kratk. Soobshch. Fiz*., **6**, 23 (2010) [*Bulletin of the Lebedev Physics Institute*, **37**, 177 (2010)].
30. Lebedev V.S., Medvedev A.S. *Kvantovaya Elektron.*, **42**, 701 (2012) [*Quantum Electron*., **42**, 701 (2012)].
31. Yoshida A., Yonezawa Y., Kometani N. *Langmuir*, **25**, 6683 (2009).
32. Yoshida A., Kometani N. *J. Phys. Chem. C*, **114**, 2867 (2010).
33. Wurtz G.A., Evans P.R., Hendren W., Atkinson R., Dickson W., Pollard R.J., Zayats A.V., Harrison W., Bower C. *Nano Lett.*, **7**, 1297 (2007).
34. Yoshida A., Uchida N., Kometani N. *Langmuir*, **25**, 11802 (2009).
35. Shapiro B.I., Kol'tsova E.S., Vitukhnovsky A.G., Chubich D.A., Tolmachev A.I., Slominskii Yu.L. *Ross. Nanotekhnol*., **6**, 83 (2011).
36. Fofang N.T., Park T.-H., Neumann O., Mirin N.A., Nordlander P., Halas N. *Nano Lett*., **8**, 3481 (2008).
37. Manjavacas A., García de Abajo F.J., Nordlander P. *Nano Lett*., **11**, 2318 (2011).
38. Walker B.J., Bulović V., Bawendi M.G. *Nano Lett*., **10**, 3995 (2010).
39. Akselrod G.M., Walker B.J., Tisdale W.A., Bawendi M.G., Bulović V. *ACS Nano*, **6**, 467 (2012).
40. Atwater H.A., Polman A. *Nat. Mater*., **9**, 205 (2010).
41. Del Puerto E., Domingo C., Sanchez-Cortes S., García-Ramos J.V., Aroca R.F. *J. Phys. Chem. C*, **115**, 16838 (2011).
42. Kim J.-B., Lee J.-H., Moon C.-K., Kim S.-Y., Kim J.-J. *Adv. Mater*., **25**, 3501 (2013)ю
43. Tanaka T., Totoki Y., Fujiki A., Zettsu N., Miyake Y., Akai-Kasaya M., Saito A., Ogawa T., Kuwahara Y. *Appl. Phys. Express*, **4**, 032105 (2011).
44. Oldenburg S.J., Averitt R.D., Westcott S.L., Halas N.J. *Chem. Phys. Lett*., **288**, 243 (1998).
45. Prodan E., Radloff C., Halas N.J., Nordlander P. *Science*, **302**, 419 (2003).
46. Brangersma M.L., Kik P.G. (Eds) *Surface Plasmon Nanophotonics* (Berlin – Heidelberg – New York: Springer-Verlag, 2007).
47. Penninkhof J.J., Moroz A., van Blaaderen A., Polman A. *J. Phys. Chem. C*, **112**, 4146 (2008).
48. Chau Y.-F., Jiang Z.-H., Li H.-Y., Lin G.-M., Wu F.-L., Lin W.-H. *Prog. Electromagn. Res. B*, **28**, 183 (2011).
49. Cole J.R., Halas N.J. *Appl. Phys. Lett*., **89**, 153120 (2006).
50. Nithyapriya M., Chellaram C. *Indian J. Innovations Dev.*, **1**, 43 (2012).
51. Mie G. *Ann. Phys. (Leipzig)*, **25**, 377 (1908).
52. Bohren C.F., Huffman D.R. *Absorption and Scattering of Light by Small Particles* (New York: Wiley, 1983).
53. Aden A.L., Kerker M. *J. Appl. Phys*., **22**, 1242 (1951).
54. Güttler A. *Ann. Phys. (Leipzig)*, **11**, 65 (1952).
55. Bhandari R. *Appl. Opt.*, **24**, 1960 (1985).
56. Wu Z.C., Wang Y.P. *Radio Sci*., **26**, 1393 (1991).
57. Sinzig J., Quinten M. *Appl. Phys. A*, **58**, 157 (1994).
58. Alù A., Engheta N. *J. Opt. A: Pure Appl. Opt*., **10**, 093002 (2008).
59. Khlebtsov N.G. *Kvantovaya Elektron*., **38**, 504 (2008) [*Quantum Electron*., **38**, 504 (2008)].
60. Qiu W., DeLacy B.G., Johnson S.G., Joannopoulos J.D., Soljačić M. *Opt. Express*, **20**, 18494 (2012).

61. Quinten M. *Optical Properties of Nanoparticle Systems: Mie and beyond* (Weinheim: Wiley-VCH Verlag GmbH & Co. KGaA, 2011).
62. Scaife B.K.P. *Principles of Dielectrics* (Oxford: Oxford Science Publ., 1998).
63. Kreibig U., Vollmer M. *Optical Properties of Metal Clusters* (Berlin: Springer, 1995).
64. Moroz A. *J. Phys. Chem. C*, **112**, 10641 (2008).
65. Khlebtsov B.N., Khlebtsov N.G. *J. Biomed. Opt.*, **11**, 44002 (2006).
66. Khlebtsov N.G. *J. Quant. Spectrosc. Radiat. Transfer*, **123**, 184 (2013).
67. Kaye G.W.C., Laby T.H. *Tables of Physical and Chemical Constants and Some Mathematical Functions* (Harlow, Essex: Longman, 1995).
68. Aspnes D.E., Studna A.A. *Phys. Rev. B*, **27**, 985 (1983).
69. Forouhi A.R., Bloomer I. *Phys. Rev. B*, **38**, 1865 (1988).